Tsunami generation by paddle motion and its interaction with a beach: Lagrangian modelling and experiment

Eugeny Buldakov

UCL, Department of Civil Engineering, Gower Street, LONDON, WC1E 6BT, UK

Abstract

A 2D Lagrangian numerical wave model is presented and validated against a set of physical wave-flume experiments on interaction of tsunami waves with a sloping beach. An iterative methodology is proposed and applied for experimental generation of tsunami-like waves using piston-type wavemaker with spectral control. Three distinct types of wave interaction with the beach are observed with forming of plunging or collapsing breaking waves. The Lagrangian model demonstrates good agreement with experiments. It proves to be efficient in modelling both wave propagation along the flume and initial stages of strongly non-linear wave interaction with a beach involving plunging breaking. Predictions of wave runup are in agreement with both experimental results and the theoretical runup law.

Keywords: Lagrangian wave modelling, tsunami run-up, wave-flume experiment

1. Introduction

Propagation of a tsunami wave approaching a coastline is a complicated process involving various physical phenomena– such as dispersion, strong nonlinearity and wave breaking– and challenging for both numerical and experimental modelling. It should be noted that the generic term "tsunami" is applied to a range of diverse wave processes requiring specific approaches. Two major mechanisms of tsunami generation– earthquakes and landslides– produce notably different waves. Earthquake tsunami generated in the deep ocean are essentially trains of very long waves of small steepness with a

typical period of hundreds of seconds (e.g. Voit, 1987). When approaching a coastline they can be treated as fast-changing tides. With dispersion hardly playing any role a basic simulation tool for propagation of earthquake tsunami in coastal regions is the nonlinear shallow water equation (Gisler, 2008). Small wave steepness compare to bathymetry gradient makes experimental scaling of these waves extremely difficult. Large scale facilities are required for adequate modelling and it is practically impossible to generate these waves at any reasonable scale using conventional types of wavemakers, e.g. piston ones. The problem had been recently solved by applying a pneumatic wave generator originally designed for tide modelling (Rossetto et al., 2011).

In this paper we consider a numerical model and an experimental methodology suitable for modelling of landslide tsunami especially those generated locally in estuaries, lakes, reservoirs and even rivers (Walder et al., 2003; Nikolkina and Didenkulova, 2012). These waves can have periods of tens of seconds, are considerably steeper and their dispersive properties cannot be neglected. A landslide tsunami is generated by fast intrusion of a large mass of solid material into a water layer. The excess of water must be accommodated by a generated wave and it is possible only if a generated wave system includes a solitary wave. The solitary wave is a well known long studied phenomenon (Miles, 1980). An important property of these waves is that for a given water depth the volume of the wave uniquely defines its energy (Longuet-Higgins and Fenton, 1974)[1]. This means that a pure solitary wave is a special case which can occur only when the perfect balance between mass and energy is maintained in the process of wave generation. Energy of two solitary waves is smaller than energy of a single wave of the same volume. Therefore, for lower energy inputs two or more solitary waves can be generated. On the other hand, the excess of energy leads to generation of an oscillating wave tail which increases the energy of the wave system without changing its volume. It should be mentioned that depression waves generated by removing a solid mass from a water layer are significantly different from compression waves described above. A depression analogue of a solitary wave does not exist and the corresponding wave represents an oscillating wave group with volume deficit provided by the set-down caused by low-frequency second-order components of the wave group spectrum. Con-

---

[1]Apart from amplitudes close to a limiting one, when a twofold relation holds

2

trary to compression waves with a high leading crest depression waves have a long leading trough of a relatively small amplitude. Such waves can for example be caused by seabed collapse.

At first glance experimental generation of a landslide tsunami should not cause problems. Indeed, starting from the work of Russell (1845) numerous experimental studies use a solitary or related waves as an object. In works specific to landslide tsunami waves are often generated using processes similar to those in nature, for example by laboratory-scale landslides (Fritz et al., 2003) or by moving underwater objects (Ataie-Ashtiani and Najafi-Jilani, 2008). This however involves design and construction of a specific facility which is not universal and can be applied only to a narrow range of problems. Yet, solitary waves can be generated by various types of wavemakers not necessarily related to natural generation mechanisms (Bukreev, 1999), e.g. by moving section of a flume bed (Hammack, 1973) or by a vertical plate moving along a flume (Goring and Raichlen, 1980). This paper considers application of a standard piston wavemaker not specifically designed for generation of such waves. The amount of energy added to water for a given displaced volume can be regulated by changing wavemaker speed for a constant value of the stroke, which allows for the generation of different wave systems of the same volume. The main problem of these simple methodologies of wave generation is that an experimentalist has very little control over the actual form of the wave. It would be beneficial to have a universal technique capable of generating arbitrary wave forms combining one or more solitary waves with a group of oscillatory waves of a pre-defined spectrum. In this paper we suggest an iterative methodology of generating tsunami-like waves in wave flumes using piston-type wavemakers with force feedback which allow precise control and partial absorption of reflected waves. The method is inspired by a similar approach used to generate focussed non-linear wave groups (e.g. Schmittner et al., 2009).

Numerical simulation of landslide tsunami implies contradictory requirements of a model. It should be capable of both accurate modelling of propagation of a dispersive wave over a complicated bathymetry and adequate representation of strongly-nonlinear wave interactions with a coastline including wave breaking. These requirements can hardly be implemented in a single model. This point can be illustrated by an example of application of the nonlinear shallow water model and the Boussinesq model to the problem of interaction of a solitary wave with a beach. The Boussinesq model is a nonlinear, weakly dispersive shallow water approximation. It can model

propagation and shoaling of a solitary wave with good accuracy. However, calculations by Boussinesq-based solvers break down when a shoaling wave approaches breaking. Stansby (2003) used a numerical filter enabling good prediction of maximum runup, but not of profiles during breaking. On the other hand the original shallow water model is non-dispersive and is unable to simulate a solitary wave, but provides a stable numerical approximation for bores and breaking waves. Borthwick et al. (2006) combined advantages of both methods using the dispersive Boussinesq model for wave propagation and the nonlinear shallow water model for wave interaction with a coastline. The same approach can be applied to more sophisticated models.

Powerful contemporary numerical models capable of simulating strongly nonlinear waves and wave breaking are based on a volume of fluid (VoF) method which can be efficiently applied for modelling of generation of landslide tsunami (Abadie et al., 2010) and their coastal interactions (Xiao and Huang, 2008). These models use a larger computational domain with cells not occupied by the fluid and introduce an artificial variable describing occupation of a cell. The boundary between fluid and air domains is not specified exactly but smoothed over several grid cells, which leads to errors in the dispersion relation. Another method recently received considerable attention is Smooth Particle Hydrodynamics (Violeau, 2012). Apart from VoF, SPH is the only method capable of modelling large scale breaking, wave impacts and slamming, and it is widely used for modelling tsunami generation, propagation and impact (e.g. Lo and Shao, 2002; Ataie-Ashtiani and Shobeyri, 2008; De Chowdhury and Sannasiraj, 2013). In SPH method approximation starts with abandoning an assumption of continuous fluid and considering individual interacting fluid particles. The method therefore does not model continuous fluid but an artificial medium which is hoped to behave like a fluid. Non-physical nature of this approximation is probably the reason why comparison of results produced by SPH models with experiments is not always perfect (e.g. Yim et al., 2008; De Padova et al., 2009; Bøckmann et al., 2012). However, progress in the development of SPH models in recent years resulted in their significant improvement (Lind et al., 2012). The main drawback of VoF and SPH models is their high requirements for computational resources. For example, Stansby et al. (2008) applied Boussinesq, VoF and SPH methods for modelling tsunami overtopping and a typical computer time for each method was 1 min, 20 hours and 50 hours respectively. Number of particles for SPH or mesh points for VoF is usually limited in practical calculations, reducing their accuracy. This makes using VoF and SPH for

modelling long-term processes impractical.

One could suggest a twofold simulation process with alternative models applied for wave propagation and coastline interaction stages. Application of a simpler and faster model with good dispersive properties at the propagation stage would allow to generate initial conditions for a more sophisticated but slow model which continues modelling to the interaction stage. It is beneficial for a simpler model to proceed as far as possible into a region of strong non-linear interactions to provide more accurate initial conditions and reduce overall modelling time. This modelling strategy was for example used by Lachaume et al. (2003) who coupled BEM and VoF methods. Boundary Element Method (BEM) solves the Laplace equation for velocity potential in the domain occupied by ideal fluid using boundary integrals. Lagrangian formulation is used to follow fluid particle trajectories on the free surface and to specify surface potential at each time step (Grilli et al., 1989, 2001). The method allows modelling steep non-breaking and overturning weaves and is considerably more efficient computationally than VoF or SPH. It is widely used by scientific and engineering communities and was successfully applied for numerous problems including ones relevant to the topic of this paper (Grilli et al., 1994; Grilli and Watts, 1999; Grilli et al., 2002). Using potential formulation restricts application of the method to irrotational flows. BEM formulation can not be applied to problems with sheared currents, which narrows area of its application.

An alternative approach is using fully Lagrangian formulation, where fluid particles are traced not only on the free surface but through the whole fluid domain. First works on finite-difference approximation of equations of fluid motion in Lagrangian formulation with applications to water wave problems appeared in early 70's. Brennen and Whitney (1970) used kinematic equations of mass and vorticity conservation for internal points of a domain occupied by ideal fluid. Flow dynamics was determined by a free-surface dynamic condition. According to Fenton (1999) this approach apparently had not been followed. It seems that there are just a few works attempting using it (e.g. Nishimura and Takewaka, 1988). Hirt et al. (1970) used momentum equations in material coordinates for describing dynamics of viscous fluid. This formulation received relatively more attention from researchers. Application of fully Lagrangian mesh models to viscous problems brings to a sharp focus their limitations. Boundary layers, wakes, vortices and other viscous effects lead to complicated deformations of fluid elements and large variations of physical coordinates over cells of a Lagrangian computational

mesh. To address this problem the method was generalised for irregular triangular meshes (Fritts and Boris, 1979) and used for development of finite element models (e.g. Ramaswamy and Kawahara, 1987) This method however remains out of the mainstream and only occasionally appears in the literature (e.g. Kawahara and Anjyu, 1988; Radovitzky and Ortiz, 1998; Staroszczyk, 2009). Finite element Lagrangian models are however complicated in both formulation and numerical realisation and are missing the main advantage expected from a Lagrangian method: simplicity of representing computational domains with moving boundaries. Simpler models can often give valuable results with less required resources. Many important water wave problems can be solved using ideal fluid model when deformation of elementary fluid volumes remains comparatively simple. These problems can be efficiently approached by much simpler Lagrangian models like the one of Brennen and Whitney (1970). In this paper we introduce a fully Lagrangian numerical model which apart from keeping other advantages of the Lagrangian approach is extremely simple and can be optimised to achieve high computational efficiency. The model can be applied to flows with an arbitrary distribution of vorticity, which makes it valuable for solving problems involving sheared currents.

As a test case for this paper we select a classical problem of interaction of a tsunami wave with a flat sloping beach, which is widely used for both numerical and experimental studies (Maiti and Sen, 1999; Lin et al., 1999; Li and Raichlen, 2001). It possesses all necessary properties required for testing the new numerical model including both wave propagation over a flat bed allowing to demonstrate dispersive properties and strongly nonlinear interaction with a sloping beach involving formation of a narrow run-up jet and consequent wave breaking. Vast amounts of analytical, numerical and experimental data are available in the literature and can be used for model validation. Probably the most useful result widely used for this purpose is an analytical relation between the height of a solitary wave and its maximum runup on a flat sloping beach suggested by Synolakis (1987).

The primary aim of the paper is developing a numerical model capable of adequate modelling of both propagation of wave systems containing solitary and dispersive components and strongly nonlinear interaction of such waves with a beach including early stages of wave breaking. Experimental work presented in this paper being used mostly for validation of the numerical model still has significance of its own. It aims to develop a methodology of generation of arbitrary wave systems including both solitary and oscillating

6

components. In section 2 we give details of the experimental set-up, describe the methodology of wave generation and experimental cases. Section 3 gives the mathematical formulation of the problem including equations of fluid motion in Lagrangian coordinates and boundary conditions. A finite-difference scheme is introduced and details of its numerical realisation are discussed. Section 4 presents comparison of experimental and numerical results and discusses interaction of waves with a beach observed in experiments and computations. Finally, section 5 summarises paper achievements and discusses ways of further development.

2. Experimental arrangements

Experiments on interaction of tsunami waves with a plain beach of $10°$ slope were performed in a coastal wave flume of the Civil Engineering department at UCL. The flume has a width of $45\,cm$ and the length of the working section is $12\,m$. The beach was installed at the left end of the flume at a distance $8.25\,m$ from a piston-type wavemaker to the toe of the slope, which is used as an origin of a coordinate system with a horizontal x-axis directed to the right towards the paddle. Water depth over the horizontal part of the bed was set to $h = 30\,cm$, which gives a position of the contact point in still water $X_c(0) = -1.701\,m$. Wave propagation was monitored by a series of resistance wave probes measuring time history of surface elevation at selected positions along the flume over both the flat bed and the beach. The schematic of the experimental layout can be seem on figure 1.

To generate a tsunami wave we require a well-controlled sharp forward or backward paddle motion. The flume paddle uses a control system operating in frequency domain and optimised for generation of oscillating waves, which cannot be directly applied for generation of tsunami. Input of the control system is the linearised amplitude spectrum of the generated wave and there is no direct control of paddle motion. The control system uses discrete spectra and generates periodic paddle motions. For our experiments we use an overall return period of $128\,sec$, which is the time between repeating identical events produced by the paddle. To provide periodicity of wavemaker motion we superimposed fast forward (backward) motions with a slow opposite motion of the same amplitude. Target paddle motions were constructed using functions of the form

$$X_{\mathrm{wm}}(t) = C\,(\,\tanh(t/T_{\mathrm{fast}}) - \tanh(t/T_{\mathrm{slow}})\,).\qquad(1)$$

Parameters C, T_{fast} and T_{slow} are selected to satisfy the following conditions: (i) the maximum speed of the slow motion is half the shallow water celerity $V_{\mathrm{slow}} = C/T_{\mathrm{slow}} = \sqrt{g\,h}/2$; (ii) the maximum speed of a combined motion $V_{\mathrm{max}} = C/T_{\mathrm{fast}} - C/T_{\mathrm{slow}}$ is a prescribed value; (iii) the total stroke $S = 2\,\mathrm{max}\,(\,X_{\mathrm{wm}}(t)\,)$ is a prescribed value. We therefore have control over two parameters: the stroke S and the maximum paddle speed V_{max}. The stroke and speed are positive if paddle moves in the direction of the wave and negative otherwise. Positive paddle motions generate compression waves with the leading crest and negative ones generate depression waves with the leading trough. Parameters of all generated paddle motions are specified in table 1.

The following iterative procedure is used to generate spectral input to the control system which would provide the desired target motion of the paddle:

$$a_{\mathrm{in}}^{n}(\omega) = a_{\mathrm{in}}^{n-1}(\omega)\,a_{\mathrm{tgt}}(\omega)/a_{\mathrm{out}}^{n-1}(\omega) = \delta_{a}^{n}(\omega)\,a_{\mathrm{tgt}}(\omega);$$
$$\phi_{\mathrm{in}}^{n}(\omega) = \phi_{\mathrm{in}}^{n-1}(\omega) + (\,\phi_{\mathrm{tgt}}(\omega) - \phi_{\mathrm{out}}^{n-1}(\omega)\,) = \phi_{\mathrm{tgt}}(\omega) + \Delta_{\phi}^{n}(\omega)\,, \qquad (2)$$

where $a_{\mathrm{in}}^{n}(\omega)$ and $\phi_{\mathrm{in}}^{n}(\omega)$ are input amplitude and phase of the spectral component at frequency ω for iteration n; $a_{\mathrm{out}}^{n}(\omega)$, $\phi_{\mathrm{out}}^{n}(\omega)$ are amplitudes and phases of the corresponding spectral components of actual paddle motion and $a_{\mathrm{tgt}}(\omega)$, $\phi_{\mathrm{tgt}}(\omega)$ are target spectral components.

The range of frequencies used in the experiments is from $1/128$ to $2\,Hz$ with 256 equally-spaced discrete frequency components. To generate initial corrections to input spectrum for the whole range of frequencies we first apply the iterative procedure (2) to a uniform spectrum of small amplitude. This gives initial corrections to input spectrum for all frequencies in the range. At the first step of the procedure we use an input spectrum identical to a target spectrum, that is a small constant amplitude for all frequency components. Target phases can be selected arbitrary and we use phases to get an unfocused target signal. The target amplitude spectrum and the corresponding signal are shown by thick solid line on figure 2. It should be noted that the methodology describes here does not depend on a particular transfer function of a wavemaker control system, which generates paddle motion from an input spectrum. Therefore, application of this methodology does not require intervention to settings of the control system and can be applied completely at user level. In our case the transfer function was generating a linear wave with the same spectrum as the input spectrum. Generation of a wave of a given amplitude requires a larger paddle stroke for a smaller frequency wave. This results in the shape of the paddle displacement spectrum presented by

8

a dashed line on the top of figure 2. The corresponding paddle movement is shown on the bottom of the figure. Then the new corrected input spectrum is calculated from the target, previous input and output spectra by applying equation (2). Initial corrections δ_a^1 and Δ_ϕ^1 obtained by this procedure can be applied to any target spectrum to generate the required input spectrum generating the target motion. Due to the linearity of the system at small amplitudes a single iteration provided satisfactory accuracy of wavemaker motion (figure 2). The initial correction gives acceptable accuracy of target paddle motions (1) for small amplitude cases and further corrections were necessary for higher amplitudes. Comparison of target paddle motions with actual ones for small and high amplitude cases is presented on figure 3. Considerable differences between real and target motions after $t = 10\,sec$ are due to reaction of the wavemaker on a wave reflected from the beach when it is being absorbed by the wavemaker.

Each of the runs specified in table 1 included 6 return periods. Record of surface elevation for the first period differs from the following ones since it starts from still water and does not include reflections observed at the beginning of each following record. The 5 following records demonstrate good level of repeatability. It was therefore assumed that the periodic wave system with the return period of $128\,sec$ is established in the flume after the first period is complete. The data for the first return period was neglected and the rest of the data was averaged between the following 5 periods. This reduces contribution of all components with periods other than the return period, that is components not originally generated by the wavemaker. This includes both high frequency noise and possible sloshing modes of the flume. It should be noted that the active absorption of reflections by the wavemaker is very efficient for low frequency waves and all reflections were absorbed before the following wave is generated. Each of the 6-period runs was repeated at least 3 times and high level of repeatability between runs was demonstrated. Interaction of a wave with the beach was filmed by a digital camcorder and wave runup on the beach was measured visually. It should be noted that runup results presented in this paper are for non-breaking or pre-breaking waves. Observed wave breaking events occur after or shortly before maximum runup and do not affect it.

3. Lagrangian water-wave formulation and numerical model

We apply a finite-difference technique directly to a 2D inviscid fully-Lagrangian water-wave formulation presented in Buldakov et al. (2006) which describes evolution of Cartesian coordinates of fluid particles $x(a, c, t)$ and $z(a, c, t)$ as a function of Lagrangian labels (a, c). The formulation can be summarised as follows. For incompressible continuous fluid the Jacobian J of the mapping $(a, c) \rightarrow (x, z)$ representing the change of an elementary volume is a motion invariant: $\partial J / \partial t = 0$. This leads to the following Lagrangian form of the continuity equation:

$$\frac{\partial(x, z)}{\partial(a, c)} = J(a, c), \tag{3}$$

where $J(a, c)$ is a given function of Lagrangian coordinates defined by initial positions of fluid particles associated with labels (a, c). The second equation can be derived from Thompson theorem on conservation of circulation around a liquid contour in ideal fluid. It follows that

$$\Omega = \nabla \times (x_t x_a + z_t z_a, x_t x_c + z_t z_c)$$

is also a motion invariant: $\partial \Omega / \partial t = 0$, where $\nabla \times$ is the curl operator in (a, c)-space. This provides us with the second kinematic condition in addition to (3)

$$\frac{\partial(x_t, x)}{\partial(a, c)} + \frac{\partial(z_t, z)}{\partial(a, c)} = \Omega(a, c), \tag{4}$$

where $\Omega(a, c)$ is a given function and for an irrotational flow $\Omega = 0$. The Lagrangian formulation does not require the kinematic free-surface condition which is satisfied by specifying a fixed curve in the Lagrangian coordinates corresponding to the free surface, e.g. $c = 0$. The dynamics of the flow is described via the dynamic free-surface condition which for the case of constant pressure on the free surface $c = 0$ has the form

$$x_{tt} x_a + z_{tt} z_a + g \, z_a \big|_{c=0} = 0. \tag{5}$$

This condition has a simple physical meaning. The left hand side of (5) can be written as a dot product of two vectors $\mathbf{a} = (x_{tt}; z_{tt} + g)$ and $\mathbf{t} = (x_a; z_a)$. The first one is the acceleration of a fluid particle with the subtracted gravity acceleration, and the second one is the vector tangential to the free surface

given in a parametric form with the parameter a. Therefore, the condition $\mathbf{a} \cdot \mathbf{t} = 0$ means that the acceleration of a fluid particle on the free surface due to its interaction with other particles (other than gravity acceleration) is normal to the free surface. The general formulation of the problem consists therefore of the continuity equation (3), the vorticity conservation equation (4), the free-surface condition (5) with suitable conditions on the bottom and side boundaries. Positions and velocities of fluid particles must be supplied as initial conditions.

A specific problem within the general formulation is defined by boundary and initial conditions. One of the advantages of Lagrangian formulation is that the choice of a Lagrangian computational domain and original correspondence between physical and Lagrangian coordinates is pretty much arbitrary and can be chosen from the consideration of convenience of numerical or analytical analysis. Practically the only restriction is that the Jacobian J of the original mapping from Lagrangian to physical coordinates $(a, c) \rightarrow (x, z)|_{t=0}$ is not singular. We use the rectangular Lagrangian domain with $c = 0$ being the free surface and $c = -h$ being the bottom, where h is some characteristic depth, for example the depth of the horizontal part of the bed in front of the beach. The horizontal coordinate of a fluid particle in the originally still water is used as the first Lagrangian label $a = x|_{t=0}$ and the second Lagrangian label is uniformly distributed between fluid particles in a vertical column from the bed to the free surface: $c = z\,h/H(x)$, where $z = -H(x)$ is the shape of the bed.

The known shape of the bottom provides the condition on the lower boundary $c = -h$ of the Lagrangian domain

$$F(\,x(a, -h, t), z(a, -h, t)\,) = 0\,, \tag{6}$$

where F is a given function. For the case of a flat bed and an inclined beach we have $F = z + h$ as $x \geq 0$ and $F = z + h + S\,x$ as $x < 0$, where S is the beach slope. On the right boundary of the Lagrangian domain $a = a_{\max}$ a given motion of a vertical wall represents the motion of a piston wavemaker:

$$x(a_{\max}, c, t) = X_{\mathrm{wm}}(t)\,, \tag{7}$$

where $X_{\mathrm{wm}}(t)$ is a prescribed motion of the paddle and we are using target motions (1) with parameters specified in Table 1. On the left boundary all Lagrangian points are mapped into a single point of a physical domain

11

representing a contact point between water surface and a beach. The corresponding condition is

$$F(\, x(a_{\min}, c, t),\ z(a_{\min}, c, t)\,) = 0 \tag{8}$$

with function F being the same as in the bottom condition (6).

The problem (3-8) was solved numerically using a finite-difference technique. Since the equations (3, 4) for internal points of the domain include only first order spatial derivatives a compact four-point Keller box scheme (Keller, 1971) can be used for finite-difference approximation of these equations. For our selection of the Lagrangian computational domain the stencil box can be chosen with sides parallel to the axes of the Lagrangian coordinate system, which significantly simplifies the final numerical scheme. Values of unknown functions x and z on the sides of the stencil box are calculated as averages of values at adjacent points and then used to approximate derivatives across the box by first-order differences. The scheme provides the second-order approximation for the central point and uses only 4 mesh points in the corners of the box which makes the resulting solver less demanding for memory resources. Time derivatives in (4) are approximated by second-order backward differences. It should be noted that the same scheme can be constructed by applying conservation of volume and circulation to elementary rectangular volumes (contours) and assuming linear behaviour of unknown functions on boundaries of the elementary volumes.

Spatial derivatives in the free-surface boundary condition (5) are approximated by second-order central differences and special attention must be paid to approximation of second time derivatives since it defines the form of the numerical dispersion relation and is crucial for the overall stability of the scheme. For simplicity let us consider a case of continuous spatial field in (3-5) combined with implicit discrete time approximation in (5). Let us approximate second derivatives by 3-point backward differences and expand this approximation to Taylor series with respect to a small time step τ. We get

$$\frac{f(t - 2\,\tau) - 2\,f(t - \tau) + f(t)}{\tau^2} = f''(t) - \tau\,f'''(t) + O(\tau^2)\,. \tag{9}$$

As can be seen the approximation is of the first order with the leading term of the error proportional to the third derivative of a function, which gives the main contribution to the error of the dispersion relation. Under an assumption of small perturbations of original particle positions we represent

unknown functions in the form

$$x = a + \varepsilon\,\xi(a, c, t); \quad z = c + \varepsilon\,\zeta(a, c, t)$$

and keep only linear terms of expansions with respect to the small displacement amplitude $\varepsilon \to 0$. Introducing a displacement potential ϕ

$$\eta = \partial\phi/\partial a; \quad \zeta = \partial\phi/\partial c$$

we satisfy the vorticity conservation (4) to the first order as $\varepsilon \to 0$ and the corresponding approximation of the continuity equation (3) is the Laplace equation for ϕ. The dynamic surface condition (5) becomes

$$\phi_a'' + g\,\phi_{ac} - \tau\,\phi_a''' = O(\tau^2)\,, \tag{10}$$

where dashes denote time derivatives and only the leading term of the approximation error from (9) is taken into account. To derive the numerical dispersion relation we are looking for a solution in the form of a regular wave in deep water:

$$\phi = e^{ika}\,e^{kc}\,e^{i\omega t}\,,$$

which satisfy the Laplace equation. The dynamic condition (10) is satisfied when a dispersion relation connecting ω and k is valid. Similar analysis can be performed for higher orders of approximation of the derivatives. Below is the summary of dispersion relations obtained for orders $n = 1 \ldots 4$:

$$\omega = \sqrt{gk}\,(\pm 1 + \frac{1}{2}\,i\,\hat{\tau} + O(\hat{\tau}^2)\,); \tag{11a}$$

$$\omega = \sqrt{gk}\,(\pm 1 \mp \frac{11}{24}\,\hat{\tau}^2 + \frac{1}{2}\,i\,\hat{\tau}^3 + O(\hat{\tau}^4)\,); \tag{11b}$$

$$\omega = \sqrt{gk}\,(\pm 1 - \frac{5}{12}\,i\,\hat{\tau}^3 + O(\hat{\tau}^4)\,); \tag{11c}$$

$$\omega = \sqrt{gk}\,(\pm 1 \pm \frac{137}{360}\,\hat{\tau}^4 - \frac{19}{24}\,i\,\hat{\tau}^5 + O(\hat{\tau}^6)\,). \tag{11d}$$

Here we use a nondimensional expansion parameter $\hat{\tau} = \sqrt{gk}\,\tau$, which is the actual measure of the problem discretisation representing the ratio of the time step to a typical problem period. As can be seen, the first-order scheme (11a) introduces numerical viscosity proportional to $\hat{\tau}$ which leads to fast non-physical decay of perturbations. The higher-order schemes (11c,11d) include terms proportional to $-i$, leading to growth of perturbations, making

13

the numerical scheme unstable. We therefore use the second-order scheme (11b), which incorporates a numerical error to dispersion at the second order $\hat{\tau}^2$ and weak dissipation at the third order $\hat{\tau}^3$. The overall numerical scheme is therefore of the second order in both time and space.

A fully-implicit time marching is applied, and Newton method is used on each time step to solve nonlinear algebraic difference equations. It is important to note that the scheme uses only 4 mesh points in the corners of a rectangular computational cell for internal points of the fluid domain. Therefore, the resulting Jacoby matrix used by nonlinear Newton iterations has a sparse 4-diagonal structure and can be effectively inverted using specific algorithms, which are considerably faster and much less demanding for computational memory than general algorithms of matrix inversion. The current version of the solver is using a standard NAG routine for inversion of general sparse matrices which does not take into account the diagonal structure of the matrix. The efficiency of the solver can be further increased by applying specialised algorithms, e.g. Thomas algorithm for block tridiagonal matrices (Thomas, 1995). To reduce calculation time inversion of a Jacoby matrix is performed at a first step of Newton iterations and if iterations start to diverge. Otherwise a previously calculated inverse Jacoby matrix is used. Usually only one matrix inversion per time step is required. An adaptive mesh is used in the horizontal direction with an algorithm based on the shape of the free surface in Lagrangian coordinates $z(a, 0, t)$ to refine the mesh at each time step in regions of high surface gradients and curvatures. Constant mesh refinement near the free surface is used in the vertical direction. Convergence tests were performed for some of the cases (figure 4). The scheme demonstrate convergence for all parameters: number of computational points in horizontal and vertical directions and time step. The convergence is good for long-wave components of a wave system, e.g. for a solitary wave component. Still, it is difficult to achieve the convergence for high frequency components especially for large computational times because of numerical errors in the dispersion relation, which are larger for high frequency waves. Compromising between accuracy and computational resources we use 201×21 computational mesh and $0.02 \, \mathrm{sec}$ time step for most calculations in the paper, which required about $5 \, \mathrm{sec}$ of computational time of a standard PC for each time step. For highly-nonlinear stages of flow with development of wave breaking a higher number of spatial points and a smaller time step were used. For example, modelling of plunging breakers required 251×31 mesh with considerable local refinement and time step of

14

0.001 s. It should be mentioned that speed of calculations was not a priority and no solver optimisation was performed to increase it.

4. Results

Waves generated during experiments are as described in section 1. Wave generated by forward paddle motions are the combinations of a non-dispersive solitary wave with oscillating wave trains. Paddle motions with equal strokes generate identical solitary wave components, with extra energy generated by faster paddle motions being carried by an oscillating dispersive wave train. Examples of the corresponding time histories of surface elevation for selected positions along the flume are presented in figures 5 and 6. Practically pure solitary waves were generated for each value of a stroke by slowest paddle motions (cases CS1V05, CS2V10 and CS3V15) while all other compressive waves include considerable dispersive tails. Most distinctively this can be observed on figure 5. Wave systems on both top and bottom plots include identical solitary waves. However, the wave generated by the faster stroke (bottom) is originally much higher because a peak of the oscillating wave tail coincides with the peak of the solitary component. Due to dispersion of the wave train and higher speed of the solitary component the height of such wave decreases fast as it propagates along the flume. Depression waves do not have a solitary component and consist of a dispersive wave train with a large leading trough and an oscillating tail. The corresponding plots for time histories of surface elevation can be seen on figure 7. A practically constant slowly increasing set-down observed on figures 5 and 6 and setup on figure 7 are due to a slow opposite component of the target wavemaker motion (1).

All experimental cases from table 1 have been simulated numerically using the model described in section 3. Comparison of the measured and computed time histories of surface elevation is presented on figures 5, 6 and 7 and demonstrates good agreement between computations and experiments. The observed discrepancies have multiple reasons both computational and experimental. The main of them are: viscous effects in the experiment, errors in the numerical dispersion relation, differences between actual and target paddle motions and gaps between the wavemaker and walls and the bed of the flume. Relative contribution of different types of errors can be observed on figure 5. The difference of heights and shape of the leading wave at the first wave probe ($x = 6.96 \, m$) is mostly due to gaps between the wavemaker and the flume walls and bed. This reduces the displaced volume and therefore

the height of the generated solitary wave. Viscous effects on the wavemaker and imperfections of wavemaker motion also contribute to this error. Viscous dissipation reduces the height of a propagation wave and results in the increasing wave height difference between inviscid computational and viscous experimental waves observed for wave probes down the flume ($x = 1.96\,m$ and $x = -1.2\,m$). The error in the numerical dispersion relation leads to a considerable accumulated error in the phase of oscillating wave trains, which can be clearly seen in the oscillating tails of the waves presented in figures 5, 6 and 7. However, the overall comparison especially for largest events within wave systems is reasonably good.

Numerical results allow to take a more detailed look into wave interaction with the beach. As demonstrated on figure 8 there are three distinctive types of such interaction. A solitary wave, which does not have a following wave train, forming a vertical wave front as the backwash interacts with the main body of water (top). The calculation process breaks down practically immediately after this. A collapsing breaker is observed in the experiment for this case, which can not be simulated by the numerical model. For a compression wave with a tail the first crest of the following wave interacts with the backwash from the beach forming a plunging breaking wave (middle). For a depression wave the following wave interacts with an uprush on the beach and exhibits a different type of plunging breaker (bottom). Both types of plunging breakers can be efficiently simulated by the model.

Compression and depression waves demonstrated considerably different forms of breakers and details of evolution of breaking waves of two types are shown on figure 9. For a compression wave the breaker is forming on an opposite current from the runup of the leading wave of the wave system. The overturning wave is created not by the progressing crest of the following wave but by the upper part of the vertical wave front created in front of the crest. The forming breaker does not move forward and overturns around a static point. This is due to the fact that the momentum of the fluid changes from negative (opposite to the wave direction) near the slope surface to positive (in the direction of the wave) near the free surface creating an angular momentum sufficient to overturn the wave front and created the breaker. It should be mentioned that this type of plunging breaking was not observed in our experiments with crushing breaking taking place instead. The probable reason for this is friction on the slope surface which reduces the negative momentum and therefore the angular momentum. The angular momentum becomes insufficient for creating the plunger, which leads to collapsing of the

vertical wave front.

Breaking of depression waves is of more conventional type. The forming breaking wave propagates into the co-directional current created by the run-up of the previous wave and the plunger is created by overturning of the wave crest, as can be observed on the right plot of figure 9. Figure 10 gives more accurate idea of the actual shapes and positions of the two types of breakers. It also shows the computational mesh in the physical domain which demonstrates deformation of fluid volume. The second breaker type was observed in the experiments and figure 11 presents comparison of experimental and calculated overturning waves of this type. Due to viscous dissipation and gaps between the wavemaker and walls and bottom of the flume in the experiment the actual wave is slightly smaller and has a different position. Therefore for comparison the experimental profiles were scaled and shifted. The scaling is the same for both snapshots on figure 11 representing different stages of breaker development. As can be seen, the shape of the calculated profile closely follows its experimental counterpart.

Wave runup can be used as a convenient integral measure of wave interaction with a beach. Synolakis (1987) suggested the following theoretical runup law for solitary waves without friction

$$R = 2.831 \, h \, \sqrt{\cot \, \beta} \, (H/h)^{5/4} \, , \tag{12}$$

where h is water depth, H is the height of a solitary wave β is the beach slope and R is the runup. This relation was confirmed by multiple experimental studies and is a good benchmark for validation of numerical models. Figure 12 shows the dependence of maximum runup with wave height determined at position $x = 1.96 \, m$ for experimental and numerical results, along with the runup law (12). Numerical and experimental points are grouped by paddle stroke. As can be expected the trend of experimental results is typical for waves with dissipation when a wave of a certain amplitude has smaller runup than its inviscid counterpart due to friction on a beach surface. Dissipative effects can also be observed in numerical results for higher amplitudes. This can be explained by small numerical viscosity of the model which produces a visible effect because of high fluid velocities in runup flows.

5. Concluding remarks

In section 1 two aims of the paper are formulated: one is numerical and another is experimental. The paper makes a significant step in achieving

17

both of these objectives. The finite-difference Lagrangian numerical model is introduced and applied to simulate a set of physical wave-flume experiments on interaction of tsunami waves with a sloping beach. An iterative methodology is used to produce experimental waves. The model demonstrates good agreement with experiments. It proves to be efficient in modelling both wave propagation along the flume and initial stages of strongly non-linear wave interaction with a beach involving plunging breaking. Predictions of wave runup are in agreement with both experimental results and the theoretical runup law by Synolakis (1987). However, there is still a considerable scope for further development.

In terms of the experimental methodology we managed to apply an iterative technique in a frequency domain to generate a fast controlled wavemaker displacement producing a solitary wave with an oscillating wave train. This however solves the problem only partially since we do not yet have control over the form of this wave train. Figure 13 gives an example of a time history and an amplitude spectrum of such a wave train obtained as a difference between signals with and without oscillating components. Our further step is therefore modification of the spectrum on figure 13 to match the desired spectrum— both amplitude and phase— of the oscillating component of the wave system. Further steps of the iterative procedure (2) can be applied to achieve this with a desired spectrum of the oscillating component being the target. The overall sequence of the wave generation process would be as follows. First, we apply the methodology described in this paper to generate a clear solitary wave and a wave train with the same solitary component but with an oscillating component of desired energy. Next, we measure time histories of surface elevation at a target position for both waves and subtract the former from the latter. The spectrum of the result is the output of the first iteration to be compared with the target. The corresponding difference of inputs to the control system gives the input of the first iteration. Then, a single step of (2) is applied and the result is added to the input of the clear solitary wave. All addition and subtraction operations are performed in the time domain. Then the procedure is repeated until (and if) it converges to desired accuracy. Such methodology opens a range of interesting opportunities in terms of modelling coastal interactions of tsunami waves since it promises generation of any combinations of oscillating waves with a solitary wave. For example, a leading oscillating component arriving before a solitary wave will modify its interaction with a beach and could lead to different runup. The ratio of a stroke of a wavemaker to water depth remains of course

the main limitation of such a technique.

A considerable advantage of the Lagrangian solver presented in the paper is its simplicity. Application of a finite-difference technique to approximate the problem (3-8) is straightforward. Choice of a rectangular Lagrangian domain with lines of computational mesh parallel to the axes of the Lagrangian coordinate system leads to a very compact numerical scheme. In most of the modern numerical water wave models using Lagrangian formulation this simplicity is overlooked. Applying complicated unstructured triangular meshes significantly complicates a discrete formulation and reduces computational efficiency. This is justified for flows in complicated physical domains which can not be continuously mapped to a rectangle or for flows with complicated vortical structure, but seems an unnecessary overcomplication for many water wave problems. However, there are situations when local mesh refinement is necessary in areas of strong free surface deformation, e.g. around a crest of a plunging breaker. An efficient solution for this problem is using a quadtree greed (e.g. Yiu et al., 1996), which is ideal for application in a rectangular Lagrangian domain and is significantly more computationally efficient than general unstructured meshes.

The results presented in the paper demonstrate model efficiency in modelling propagation of tsunami-like waves and initial stages of their interaction with a shore. Still, improvement of the numerical dispersion relation and further reducing numerical viscosity is advisable. Fortunately, this is possible without significant complication of the model. Using the fourth-order approximation of second time-derivatives in the dynamic condition (5) would give better results in terms of both accuracy and faster convergence if not for the unstable fifth-order term in the numerical dispersion relation (11d). To remove this instability we can include a dissipative term proportional to τ^4 to the dynamic boundary condition:

$$x_{tt}x_a + z_{tt}z_a + g\,z_a + k\,\tau^4\,(x_t x_a + z_t z_a + g\,z_a)\,|_{c=0} = 0\,.$$

The term in brackets describes an artificial resistance to surface motion and parameter k should be selected to compensate for the unstable term in (11d). The resulting stable numerical scheme will have fourth order in time. It will allow for eliminating numerical viscosity and considerably reducing phase error accumulated by propagating wave trains.

In general we can conclude that the Lagrangian solver demonstrates great potential in modelling generation, propagation and shoaling of tsunami waves.

19

References

Abadie, S., Morichon, D., Grilli, S., Glockner, S., 2010. Numerical simulation of waves generated by landslides using a multiple-fluid Navier-Stokes model. Coastal Engineering 57 (9), 779–794.

Ataie-Ashtiani, B., Najafi-Jilani, A., 2008. Laboratory investigations on impulsive waves caused by underwater landslide. Coastal Engineering 55 (12), 989 – 1004.

Ataie-Ashtiani, B., Shobeyri, G., 2008. Numerical simulation of landslide impulsive waves by incompressible smoothed particle hydrodynamics. International Journal for Numerical Methods in Fluids 56 (2), 209–232.

Bøckmann, A., Shipilova, O., Skeie, G., 2012. Incompressible SPH for free surface flows. Computers and Fluids 67, 138–151.

Borthwick, A., Ford, M., Weston, B., Taylor, P., Stansby, P., 2006. Solitary wave transformation, breaking and run-up at a beach. Proceedings of the Institution of Civil Engineers: Maritime Engineering 159 (3), 97–105.

Brennen, C., Whitney, A. K., 1970. Unsteady, free surface flows; solutions employing the Lagrangian description of the motion. In: 8th Symposium on Naval Hydrodynamics. Office of Naval Research, pp. 117–145.

Bukreev, V. I., 1999. Correlation between theoretical and experimental solitary waves. Journal of Applied Mechanics and Technical Physics 40, 399–406.

Buldakov, E. V., Eatock Taylor, R., Taylor, P. H., 2006. New asymptotic description of nonlinear water waves in Lagrangian coordinates. J. Fluid Mech. 562, 431–444.

De Chowdhury, S., Sannasiraj, S., 2013. SPH simulation of shallow water wave propagation. Ocean Engineering 60, 41–52.

De Padova, D., Dalrymple, R. A., Mossa, M., Petrillo, A. F., 2009. SPH simulations of regular and irregular waves and their comparison with experimental data. arXiv preprint arXiv:0911.1872.

Fenton, J. D., 1999. Numerical methods for nonlinear waves. Advances in coastal and ocean engineering 5, 241–324.

Fritts, M., Boris, J., 1979. The Lagrangian solution of transient problems in hydrodynamics using a triangular mesh. Journal of Computational Physics 31 (2), 173–215.

Fritz, H., Hager, W., Minor, H.-E., 2003. Landslide generated impulse waves. Experiments in Fluids 35 (6), 505–519.

Gisler, G., 2008. Tsunami simulations. Annual Review of Fluid Mechanics 40, 71–90.

Goring, D., Raichlen, F., 23–28 March 1980. The generation of long waves in the laboratory. In: Seventeenth Coastal Engngineering Confference. Sydney, Australia.

Grilli, S., Guyenne, P., Dias, F., 2001. A fully non-linear model for three-dimensional overturning waves over an arbitrary bottom. International Journal for Numerical Methods in Fluids 35 (7), 829–867.

Grilli, S., Skourup, J., Svendsen, I., 1989. An efficient boundary element method for nonlinear water waves. Engineering Analysis with Boundary Elements 6 (2), 97–107.

Grilli, S., Subramanya, R., Svendsen, I., Veeramony, J., 1994. Shoaling of solitary waves on plane beaches. Journal of Waterway, Port, Coastal, & Ocean Engineering - ASCE 120 (6), 609–628.

Grilli, S., Vogelmann, S., Watts, P., 2002. Development of a 3D numerical wave tank for modeling tsunami generation by underwater landslides. Engineering Analysis with Boundary Elements 26 (4), 301–313.

Grilli, S., Watts, P., 1999. Modeling of waves generated by a moving submerged body. applications to underwater landslides. Engineering Analysis with Boundary Elements 23 (8), 645–656.

Hammack, J. L., 1973. A note on tsunamis: their generation and propagation in an ocean of uniform depth. Journal of Fluid Mechanics 60 (04), 769–799.

Hirt, C., Cook, J., Butler, T., 1970. A Lagrangian method for calculating the dynamics of an incompressible fluid with free surface. Journal of Computational Physics 5 (1), 103 – 124.

Kawahara, M., Anjyu, A., 1988. Lagrangian finite element method for solitary wave propagation. Computational Mechanics 3 (5), 299–307.

Keller, H. B., 1971. A new difference scheme for parabolic problems. In: Numerical Solution of Partial Differential Equations, II (SYNSPADE 1970) (Proc. Sympos., Univ. of Maryland, College Park, Md., 1970). Academic Press, New York, pp. 327–350.

Lachaume, C., Biausser, B., Grilli, S., Frauni, P., Guignard, S., 2003. Modeling of breaking and post-breaking waves on slopes by coupling of BEM and VOF methods. In: Proceedings of the International Offshore and Polar Engineering Conference. pp. 1698–1704.

Li, Y., Raichlen, F., 2001. Solitary wave runup on plane slopes. Journal of Waterway, Port, Coastal and Ocean Engineering 127 (1), 33–44.

Lin, P., Chang, K.-A., Liu, P.-F., 1999. Runup and rundown of solitary waves on sloping beaches. Journal of Waterway, Port, Coastal and Ocean Engineering 125 (5), 247–255.

Lind, S., Xu, R., Stansby, P., Rogers, B., 2012. Incompressible smoothed particle hydrodynamics for free-surface flows: A generalised diffusion-based algorithm for stability and validations for impulsive flows and propagating waves. Journal of Computational Physics 231 (4), 1499–1523.

Lo, E., Shao, S., 2002. Simulation of near-shore solitary wave mechanics by an incompressible SPH method. Applied Ocean Research 24 (5), 275–286.

Longuet-Higgins, M. S., Fenton, J. D., 1974. On the mass, momentum, energy and circulation of a solitary wave. II. Proceedings of the Royal Society of London. A. Mathematical and Physical Sciences 340 (1623), 471–493.

Maiti, S., Sen, D., 1999. Computation of solitary waves during propagation and runup on a slope. Ocean Engineering 26 (11), 1063–1083.

Miles, J. W., 1980. Solitary waves. Annual Review of Fluid Mechanics 12 (1), 11–43.

Nikolkina, I., Didenkulova, I., 8–10 May 2012. River landslides in Nizhny Novgorod region and a possibility of local tsunami generation. In: Baltic International Symposium (BALTIC), 2012 IEEE/OES. Klaipeda, Lithuania.

Nishimura, H., Takewaka, S., 1988. Numerical analysis of two-dimensional wave motion using lagrangian description. Doboku Gakkai Rombun-Hokokushu/Proceedings of the Japan Society of Civil Engineers 9 (5), 191–199, in Japanese.

Radovitzky, R., Ortiz, M., 1998. Lagrangian finite element analysis of newtonian fluid flows. International Journal for Numerical Methods in Engineering 43 (4), 607–619.

Ramaswamy, B., Kawahara, M., 1987. Lagrangian finite element analysis applied to viscous free surface fluid flow. International Journal for Numerical Methods in Fluids 7 (9), 953–984.

Rossetto, T., Allsop, W., Charvet, I., Robinson, D., 2011. Physical modelling of tsunami using a new pneumatic wave generator. Coastal Engineering 58 (6), 517–527.

Russell, J., 1845. Report on Waves. John Murray, London, pp. 311 – 390, Report on the Fourteenth Meeting of the British Association for the Advancement of Science; Held at York in September 1844.

Schmittner, C., Kosleck, S., Hennig, J., May 31– June 5 2009. A phase-amplitude iteration scheme for the optimization of deterministic wave sequences. In: Proceedings of the International Conference on Offshore Mechanics and Arctic Engineering - OMAE. Honolulu, Hawaii, USA.

Stansby, P., 2003. Solitary wave run up and overtopping by a semi-implicit finite-volume shallow-water boussinesq model. Journal of Hydraulic Research 41 (6), 639–647.

Stansby, P., Xu, R., Rogers, B., Hunt, A., Borthwick, A., Taylor, P., 30 September–2 October 2008. Modelling tsunami overtopping of a sea defence by shallow-water boussinesq, VOF and SPH methods. In: Proceedings of the European Conference on Flood Risk Management Research Into Practice (FLOODRISK 2008). Oxford, UK.

Staroszczyk, R., 2009. A Lagrangian finite element analysis of gravity waves in water of variable depth. Archives of Hydroengineering and Environmental Mechanics 56 (1-2), 43–61.

Synolakis, C. E., 1987. The runup of solitary waves. J . Fluid Mech. 185, 523–545.

Thomas, J. W., 1995. Numerical Partial Differential Equations: Finite Difference Methods. Springer-Verlag, New York.

Violeau, D., 2012. Fluid Mechanics and the SPH Method: Theory and Applications. Oxford University Press, Oxford.

Voit, S., 1987. Tsunamis. Annual Review of Fluid Mechanics 19, 217–236.

Walder, S., Watts, P., Sorensen, O., Janssen, K., 2003. Tsunamis generated by subaerial mass flows. Journal of Geophysical Research B: Solid Earth 108 (B5), 2236.

Xiao, H., Huang, W., 2008. Numerical modeling of wave runup and forces on an idealized beachfront house. Ocean Engineering 35 (1), 106 – 116.

Yim, S., Yuk, D., Panizzo, A., Di Risio, M., Liu, P.-F., 2008. Numerical simulations of wave generation by a vertical plunger using rans and SPH models. Journal of Waterway, Port, Coastal and Ocean Engineering 134 (3), 143–159.

Yiu, K., Greaves, D., Cruz, S., Saalehi, A., Borthwick, A., 1996. Quadtree grid generation: Information handling, boundary fitting and CFD applications. Computers & Fluids 25 (8), 759 – 769.
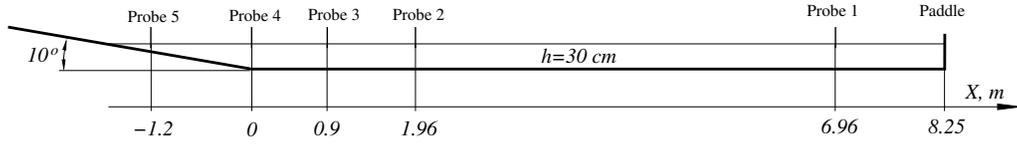
Figure 1: Wave flume layout and positions of wave probes

Wave Type	Case name	Paddle stroke: S/h	Max paddle speed: $V/\sqrt{g\,h}$
	CS1V05	1/3	5
	CS1V10	1/3	10
	CS1V15	1/3	15
	CS2V10	2/3	10
Compression	CS2V15	2/3	15
	CS2V20	2/3	20
	CS3V20	1	20
	CS3V25	1	25
	CS3V30	1	30
	DS1V15	1/3	15
Depression	DS2V20	2/3	20
	DS3V25	1	25

Table 1: Experimental and computational cases
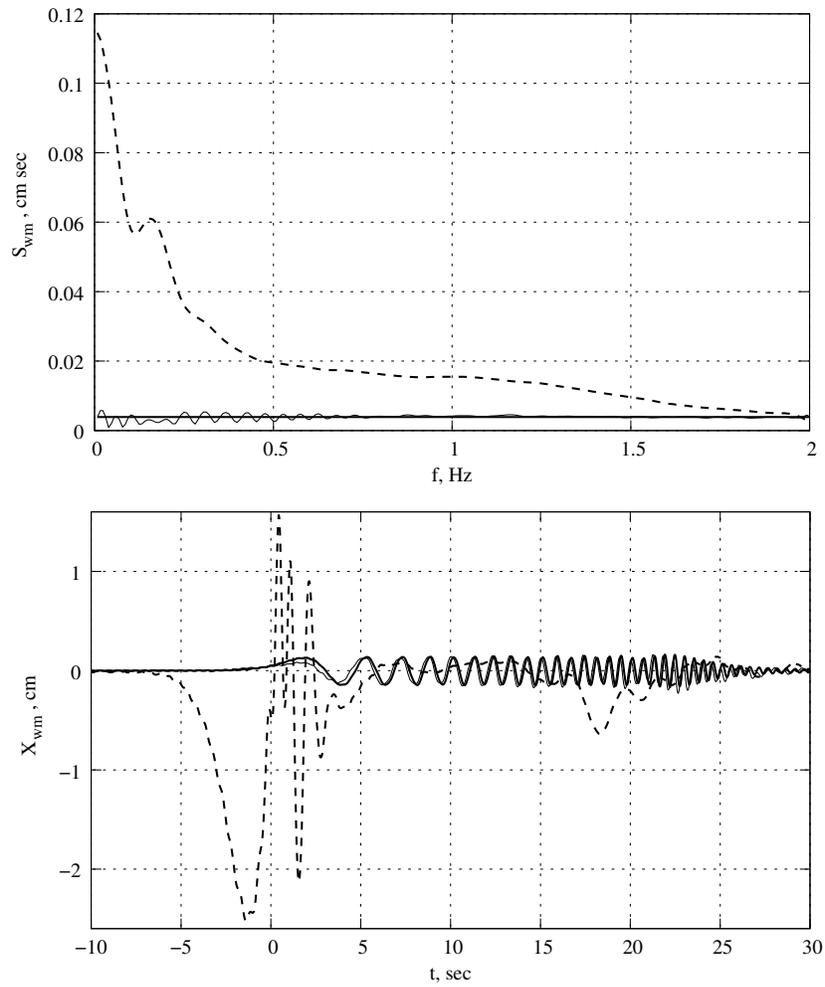
Figure 2: Initial correction of wavemaker displacement. Before correction (dashed), after correction (thin solid), target (thick solid). Amplitude spectrum (top), wavemaker position (bottom).

26
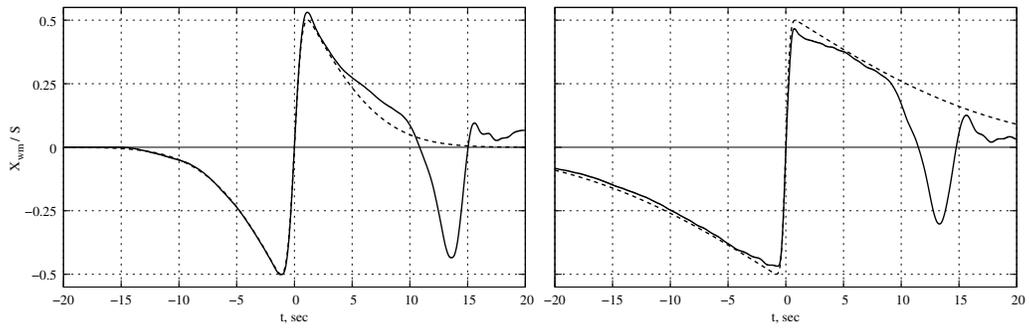
Figure 3: Time history of wavemaker displacement for cases CS1V05 (left) and CS3V25 (right). Target (dashed) and actual (solid) paddle motions.
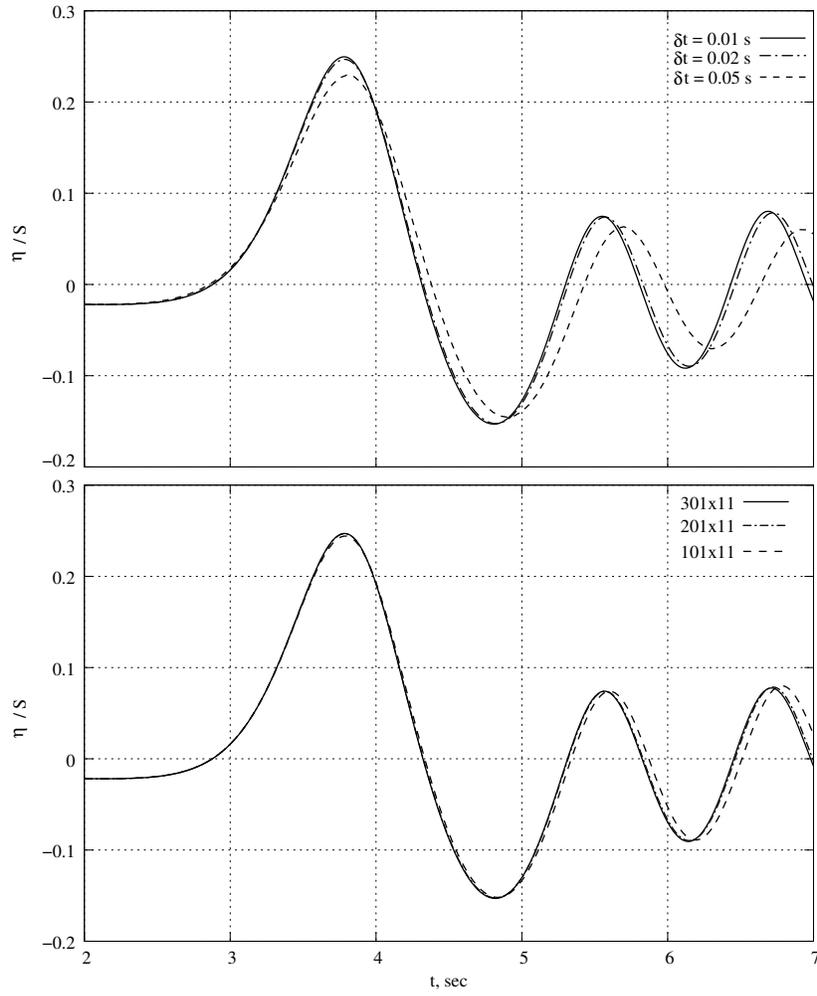
Figure 4: Convergence of numerical results for time history of surface elevation at positions $x = 1.96\,m$ for the case CSV15. Top – 201×11 mesh, decreasing time step; Bottom – $deltat = 0.02\,s$, increasing number of points in horizontal direction.
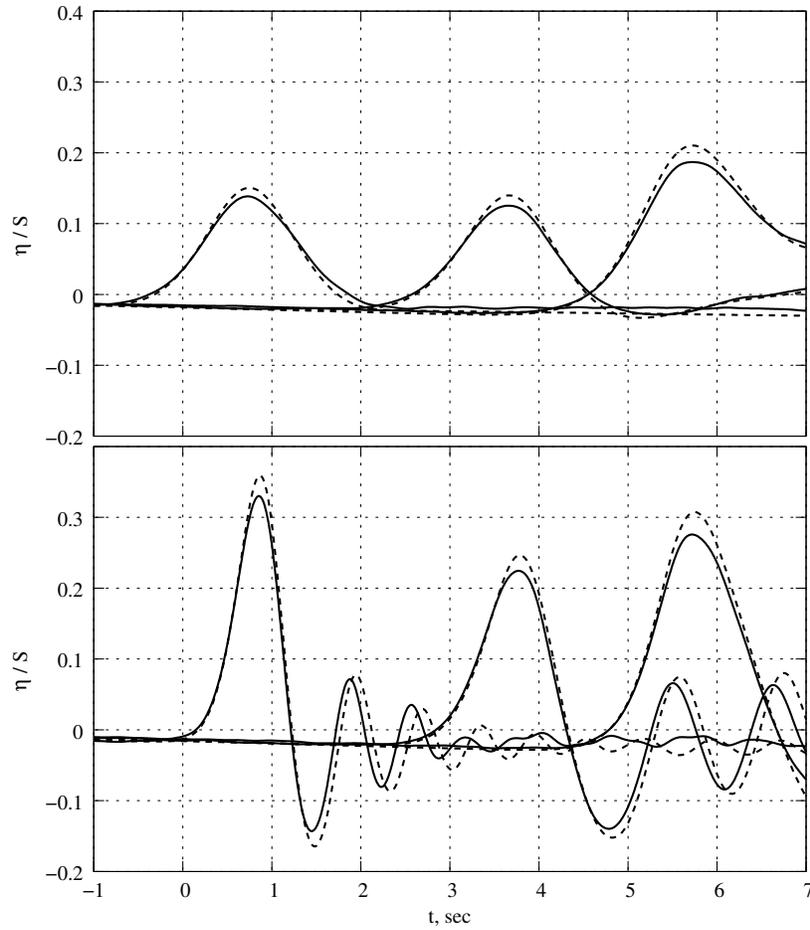
Figure 5: Time histories of surface elevation of compression waves of small amplitude at positions $x = 6.96\,m$; $x = 1.96\,m$ and $x = -1.2\,m$ for experiment (solid) and computations (dashed). Non-dispersive wave, case CS1V05 (top); dispersive wave, case CS1V15 (bottom).

29
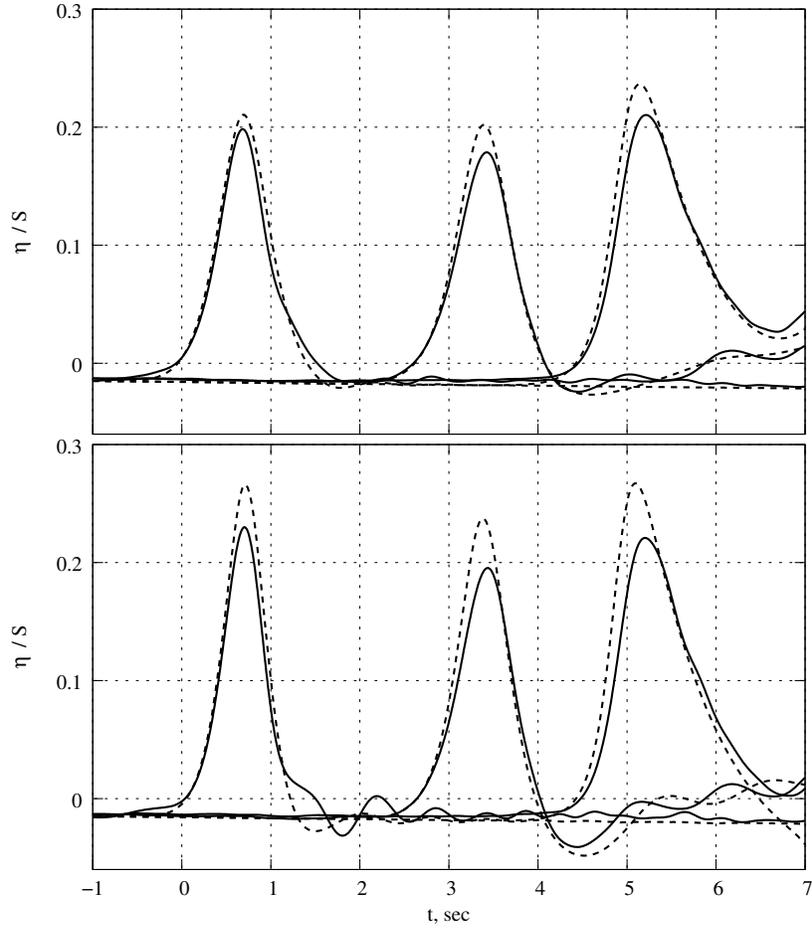
Figure 6: Time histories of surface elevation of compression waves of large amplitude at positions $x = 6.96\,m$; $x = 1.96\,m$ and $x = -1.2\,m$ for experiment (solid) and computations (dashed). Non-dispersive wave, case CS1V05 (top); dispersive wave, case CS1V15 (bottom).
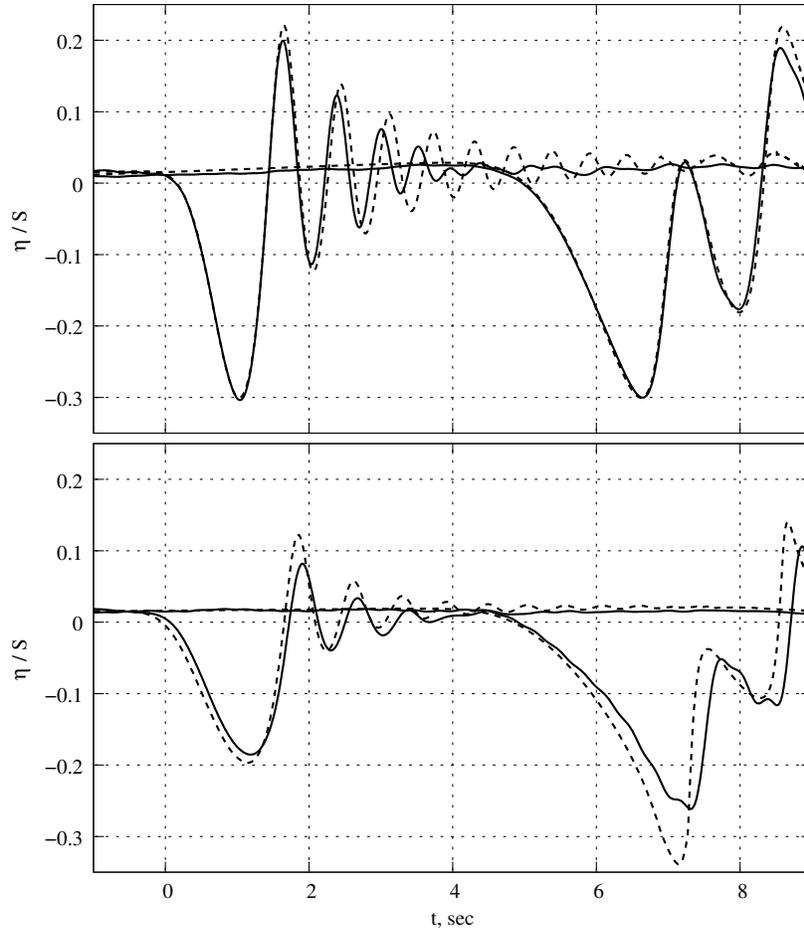
Figure 7: Time histories of surface elevation of depression waves at positions $x = 6.96\,m$ and $x = -1.2\,m$ for experiment (solid) and computations (dashed). Small amplitude wave, case DS1V15 (top); large amplitude wave, case DS3V25 (bottom). The elevation is scaled by paddle stroke.
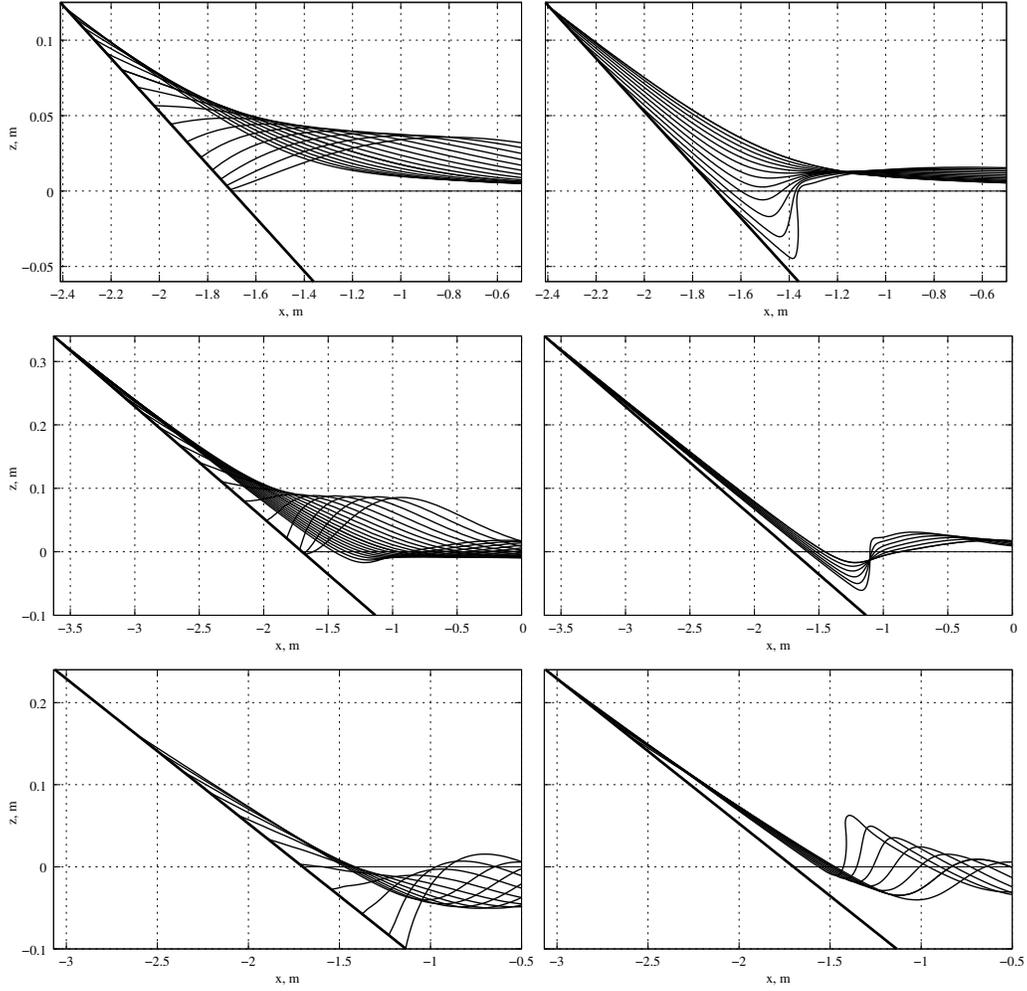
Figure 8: Types of wave interaction with a sloping beach. Top– solitary wave, case CS2V10: running up (left); running down (right). Middle– compression wave with a following wave train, case CS3V30: running up (right); running down against a following wave (right). Bottom– depression wave, case DS3V25: running up (left); running up with a following wave. Time step between contours is 0.1 sec.
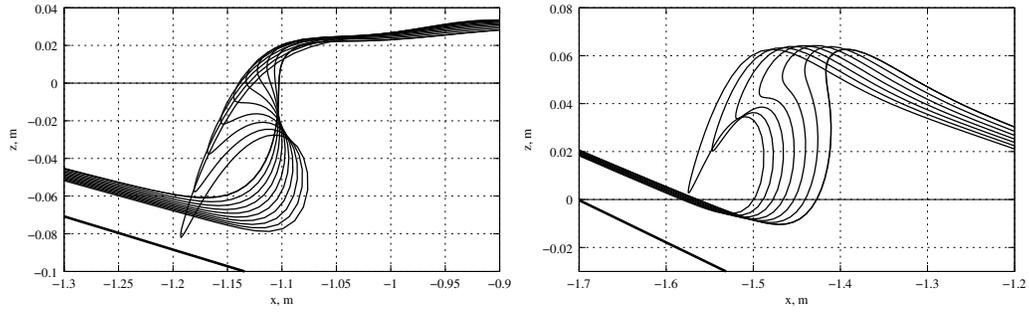
Figure 9: Forming of plunging breakers by following waves on running-down (left, case CS3V30) and and running-up (right, case DS3V25) flows. Time step between contours is 0.02 sec.
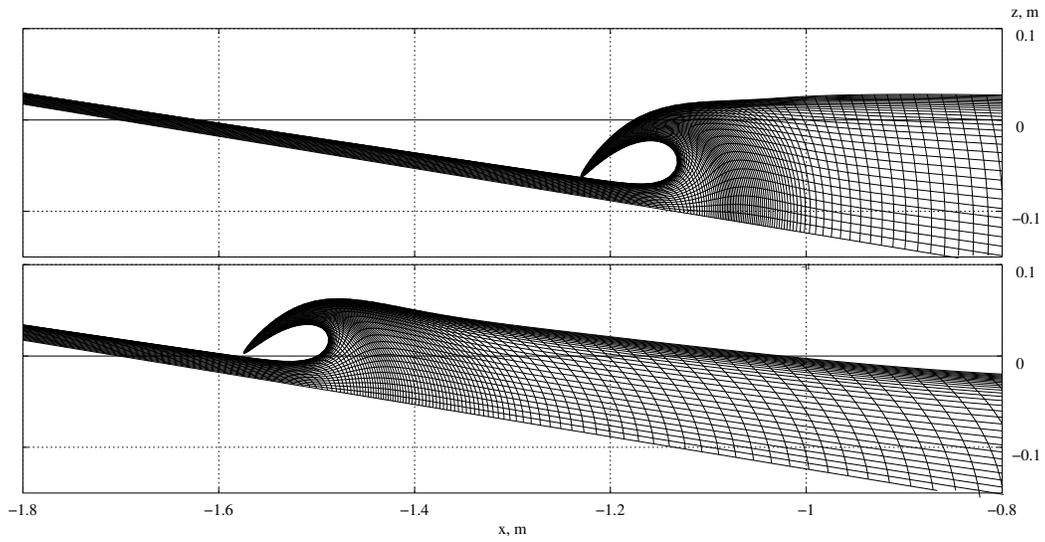
Figure 10: Two types of plunging breakers: compression wave, case CS3V25 (top); depression wave, case DS3V25 (bottom).
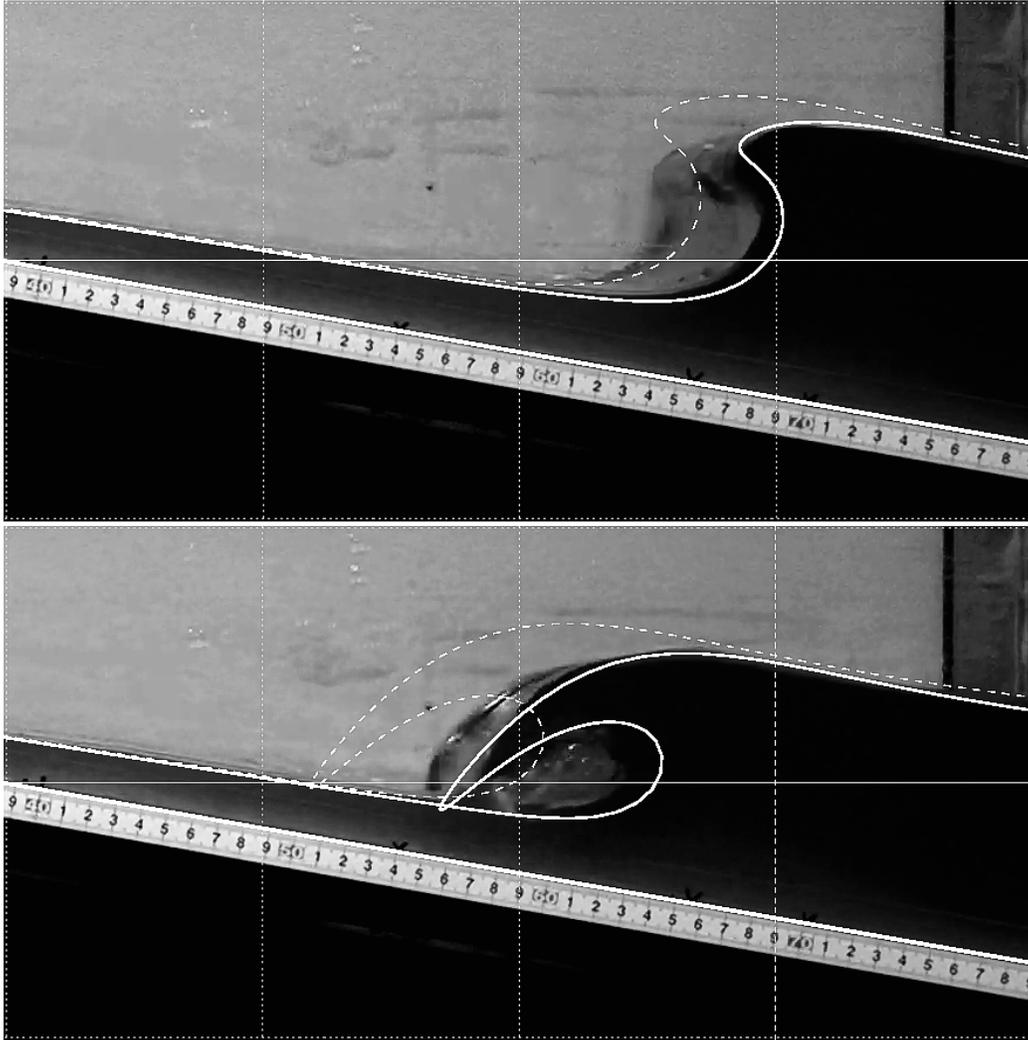
Figure 11: Comparison between calculated and experimental profiles of a plunging breaker. Case DS3V25. Dashed– actual calculated profiles. Solid– scaled and shifted calculated profiles (scale factor 0.95). Time between snapshots is 0.1 sec
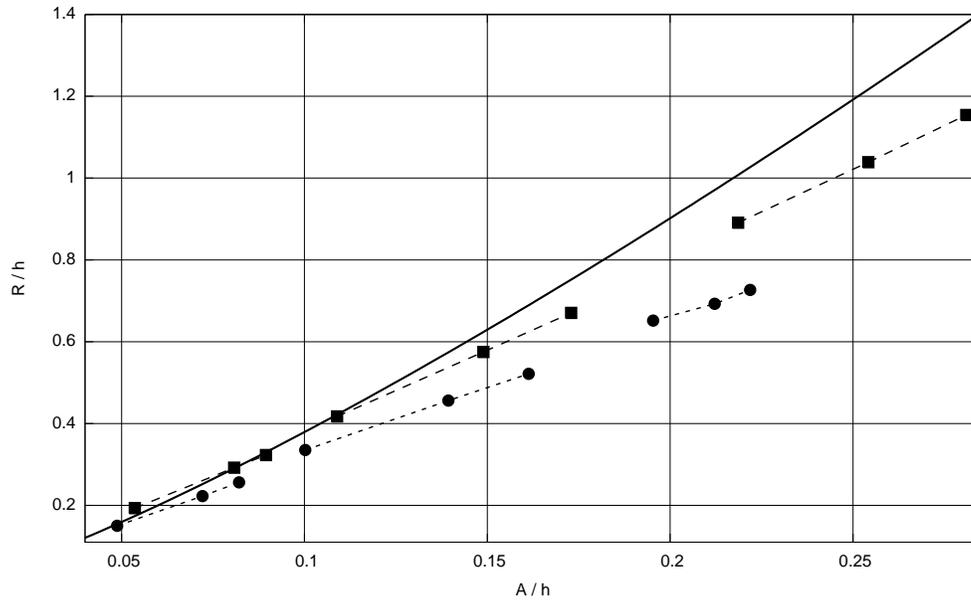
Figure 12: Dependence of wave run-up on its maximum elevation at position $x = 1.96\,m$. Squares– calculations; circles– experiment. Cases are grouped by paddle stroke. Solid line represents the runup law (12).
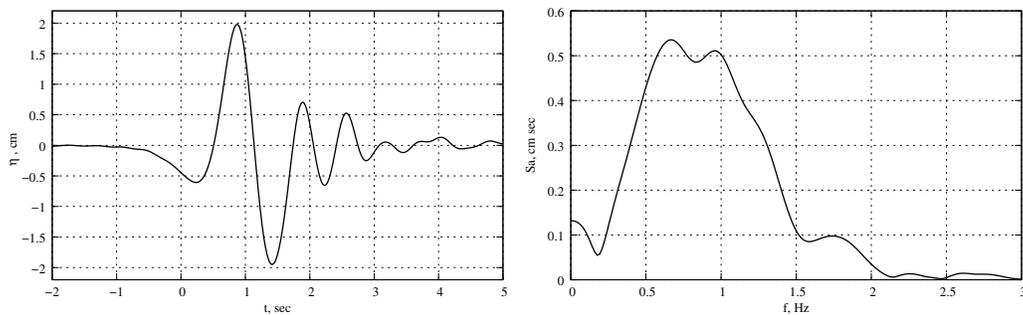

Figure 13: Experimental surface elevation of an oscillating wave train component at position $x = 6.96\,m$ for the case CS1V15 obtained by subtracting the signal for the case CS1V10 (solitary wave) from the full signal of CS1V15. Time history (left) and amplitude spectrum (right).